Journal of Mines and Geosciences
ISSN 3057-3483

Mafic related Metallic Mineral Deposits in the Msangano Trough, Mbozi Terrane, Tanzania: Insights from Apparent Density Mapping

Kelvin K Kayuni

Department of Geoscience, University of Dar es Salaam, P.O. Box 35052, Dar es Salaam, Tanzania.

**Corresponding author: kelvinkayuni13@gmail.com*

Keywords

Msangano Trough; Mughese Shear Zone; TOPEX Gravity; Apparent Density; Metallic Mineral Deposits

Article information

Submitted:
1st January 2025
Reviewed:
25th March 2025
Accepted: 9th April 2025
Publ. 19th May 2025

Abstract

This study reports the occurrence of mafic-related metallic mineral deposits in the Msangano Trough of the Mbozi terrane, Tanzania. The study investigated the Msangano Trough by applying apparent density mapping and edge detection methods to TOPEX gravity data of the study area, utilizing Oasis Montaj software. The edge detectors were used to locate contacts, and faults, and, to calculate depths to the gravity anomalies. The apparent density values were utilized to distinguish metallic mineral deposits from non-mineralized intrusions. The results from these methods were combined to construct the structural map of the study area. The results show that the area is structurally controlled by major faults predominantly trending in the northwest-southeast direction. The area has two metallic mineral deposits, A and B, with density values ranging from 3.62 to 4.30 g/cm^3. These deposits, A and B, span 109.8 and 62.2 km^2, respectively. The Euler deconvolution and Direct Source Parameter Imaging indicate that the deposits are situated at an average depth of 950 m below the surface. The age of the basalts in the Mbozi terrane correlates well with the age of the Bushveld Igneous Complex in South Africa and the Sudbury Complex in Ontario, Canada. This indicates that the Msangano deposits, the Bushveld Igneous Complex, and the Sudbury Complex were all emplaced during the same era of magmatic events. This suggests that the Msangano trough is a promising area for the exploration and prospecting of metallic minerals such as chromium, platinum group metals, or nickel, which are also enriched in the Bushveld Igneous Complex and the Sudbury Complex. Additionally, the findings provide crucial information that can guide further exploration of metallic mineral deposits in the Msangano Trough and adjacent areas.

1. Introduction and Background

The study area is situated in southwestern Tanzania, encompassing the eastern part of the Ufipa Plateau, the Msangano Trough, and the northern part of the Mbozi block (Figure. 1). The total size of the study area is 2024 km^2. About one-fourth of the study area (the western part) is occupied by the Ufipa plateau, while the remaining part (the Msangano Trough and Mbozi block) falls within the Mbozi terrane (Figure. 2). The study area is characterized by highlands, lowlands (including the Msangano Trough, and Utambalila- Ipapa Basin), and perennial rivers (Figure. 2).

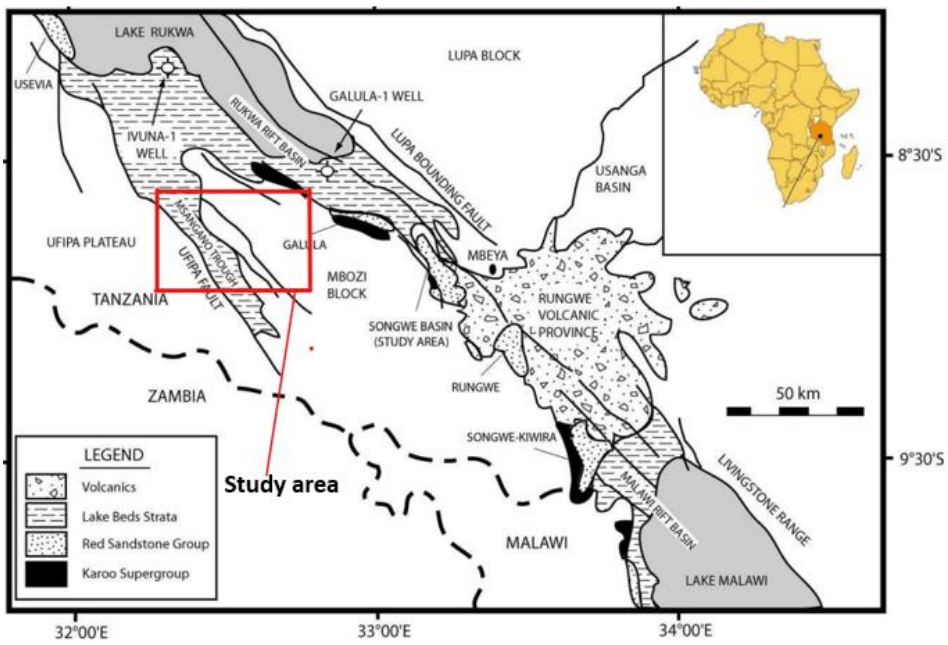

Figure. 1: Map of southwestern Tanzania showing the location of the study area. Modified from Damblon et al. (1998).

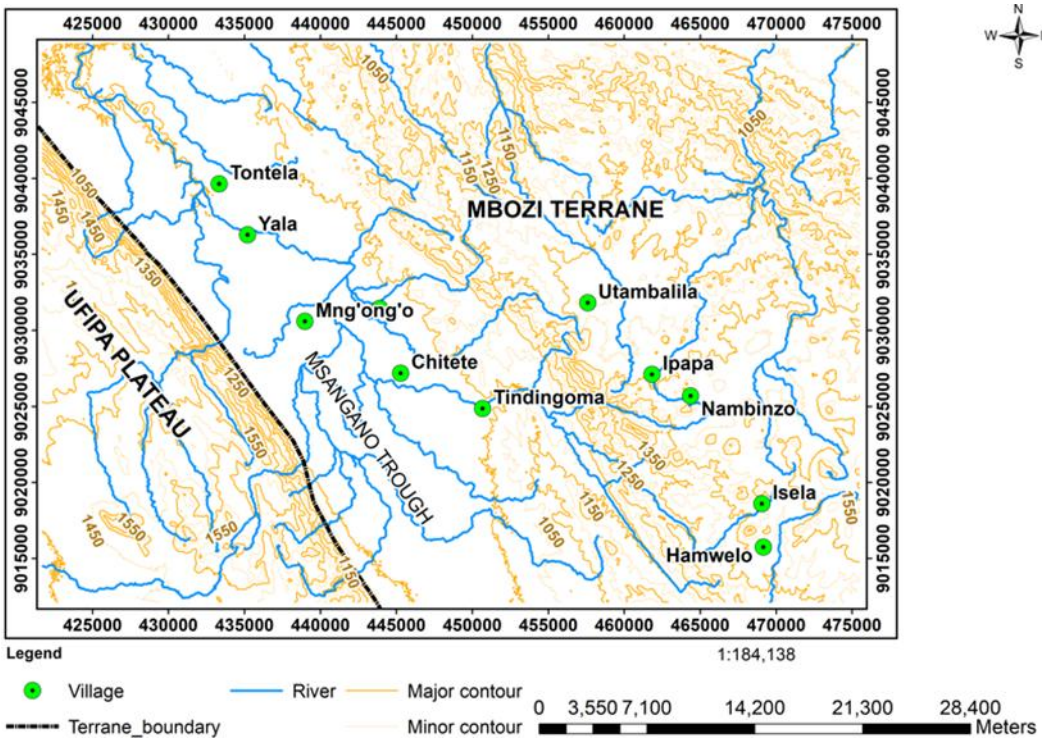

Figure. 2: Topographic map of the study area.

The study area is characterized by Paleoproterozoic metasediments, meta-igneous rocks, gneiss, migmatite, amphibolite, and quartzite (Pinna et al., 2004; Figure 3). The Mbozi terrane predominantly consists of Paleoproterozoic Meta-basalts rocks that are approximately 1977 ± 40 Ma old (Boven et al., 1999; Boniface, 2009). Late Cenozoic fine clastic sediments cover the Msangano Trough, while sandy, gravelly, and silt sediments occur in the small part of the Mbozi block (Pinna et al., 2004). The Msangano Trough is bordered by northeast and southwest dipping Cenozoic faults (Morley et al., 1992). On the west side, the Msangano Trough is

bordered by the Ufipa Fault (Figure.1). The Msangano Trough is also a part of the Rukwa Rift (Daly, 1988; Lenoir et al., 1994; Delvaux et al., 2012; Lemna et al., 2019).

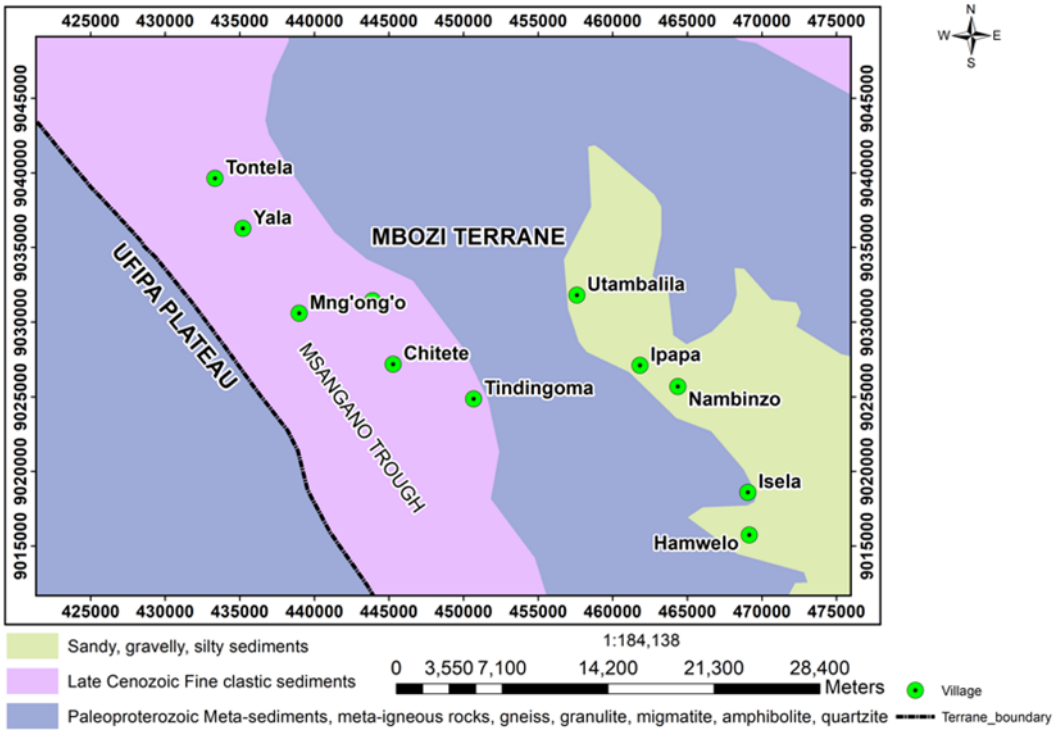

Figure. 3: Geological map of the study area showing the dominant lithologies. Modified from Pinna et al. (2004).

Previous regional geophysical investigations involved interpretation of aeromagnetic and seismic reflection datasets (Kilembe & Rosendahl, 1992; Kolawole et al., 2021). The aeromagnetic study by Kolawole et al. (2021) reported the occurrence of high magnetic anomalies in the region. These high magnetic anomalies were interpreted as the Chisi and Mughese shear zones. The Chisi shear zone is dominated by steep, northeast-southwest dipping, metamorphic fabrics hosted by eclogite facies rocks. The Mughese shear zone is 15 km wide and located beneath the Msangano Trough. Kolawole et al. (2021) failed to study the Mughese shear zone due to the lack of relevant data. The interpretation of seismic reflection data by Kilembe and Rosendahl (1992) was based on 2050 line-km of multifold seismic reflection data spaced at 4 km intervals, and was primarily intended to investigate the structure and stratigraphy of the Rukwa rift for the Hydrocarbon exploration, rather than metallic mineral deposits prospecting which is the purpose of this study.

The mafic terranes are potential areas for prospecting metallic mineral deposits related to mafic intrusions (Gilbert & Park, 2007). The mafic intrusions are famous for hosting Nickle and Platinum group elements ore deposits (Wadsworth et al., 1982). Given that mafic sequences are dominating the Mbozi terrane, which is being studied here, then the Mughese shear zone beneath the Msangano Trough forms a potential metallic mineral deposits target associated with the mafic- intrusions. This is because the magmatic-related metallic mineral deposits find their way toward deposition in the subsurface or near the surface via weak zones such as fault and shear zones. This was the primary reason for conducting this study: to investigate the Msangano Trough.

The investigation of the Msangano Trough for the occurrence of mafic-related metallic mineral deposits by this study was also inspired by the known occurrence of similar deposits and prospects in the neighboring terranes, particularly in the Lupa terrane, which are structurally controlled or hosted by steeply south-dipping D2 (Second deformation) quartz veins and greenschist facies mylonitic shear zones. The majority of these are associated with the east-northeast to west-southwest trending Saza shear

zone and two other dominant structural trends, northwest-southeast and east-west (Lawley et al., 2014). Despite the geological differences between the Lupa terrane which is dominated by Granitic gneisses, and the Mbozi terrane which is dominated by Meta-basalts (Grantham, 1931; Boven et al., 1999; Boniface, 2009). The presence of shear zones controlling gold mineralization in the Lupa terrane suggests that the Mughese shear zone in the Mbozi terrane may also have potential for metallic mineral deposit.

The metallic mineral deposits are always denser than the surrounding rocks in any area of their occurrence; they may occur as intrusions with high gravity anomaly in the weak zones such as faults or shear zones. The high-density property of these types of deposits is caused by the presence of dense minerals such as platinum group metals, sulfides group, precious minerals, oxides, and silicate minerals. The average density values of metallic minerals range from 2.45 to 7.5 g/cm^3, with the platinum group metals reaching a higher density of 19 g/cm^3. In contrast, the density of the normal rocks varies from 1.96 g/cm^3 (Alluvium) to 3.54 g/cm^3 density of Eclogite (Kearey et al., 2002; Yadav & Sircar, 2019). Therefore, this study defines the mafic-related metallic deposit as any intrusion (Present in the study area) with an average density value greater than 3.54 g/cm^3.

Due to their high-density values compared to the surrounding rocks, any buried metallic mineral deposits occurring in the study area can easily be mapped using the apparent density mapping technique from gravity data. The apparent density mapping by applying an inverse density deconvolution filter to the residual Bouguer Anomaly gives density values for the upper crust which correspond well with the averaged density values from the rock samples (Granser et al., 1989).

Therefore, the main objective of this study is to investigate the occurrence of metallic mineral deposits linked to continental mafic intrusions within the Msangano Trough of the Mbozi terrane, Tanzania. By utilizing the apparent density mapping technique, interpretation of the TOPEX gravity data of the study area revealed the presence of two metallic mineral deposits within the Msangano Trough. These findings, which will be detailed and discussed in the following sections, provide new insights into metallic prospecting and exploration in the Msangano Trough and the Mbozi Terrane in general.

2 Material and Methods

Two primary datasets were employed to accomplish the focus of this study. They include TOPEX gravity satellite and Digital Elevation Model from the Shuttle Radar Topography Mission (DEM SRTM) datasets.

This study used an apparent density mapping technique and edge detectors on the TOPEX gravity satellite data to identify and locate metallic mineral deposits, contacts, and subsurface faults in the study area. The TOPEX gravity satellite data was downloaded through https://topex.ucsd.edu/cgi-bin/get_data.cgi.

The Digital Elevation Model from the Shuttle Radar Topography Mission (DEM SRTM) was processed using ArcGIS (ArcMap), Arc SWAT, Global mapper and RockWorks17 software to study the topography of the study area, and orientation of the surface geological structures (surface lineaments). The DEM SRTM data was downloaded from the United States Geological Survey (USGS) website through https://earthexplorer.usgs.gov/.

The TOPEX satellite provides Free Air Anomaly (FAA) data, the distance between data points is 1.8 km, and the data has been automatically corrected with Latitude correction, Drift correction, and Tidal correction (Siombone et al., 2022). 630 FAA point data were used in this study. The obtained FAA was then processed using Oasis Montaj software.

The processing of the FAA data involved the following steps: Terrane Correction (TC), Bouguer Anomaly (BA), Complete Bouguer Anomaly (CBA), Local density calculation, separation of residual Bouguer Anomaly, regional Bouguer Anomaly and noise from Complete Bouguer Anomaly (CBA).This was followed by the downward continuation of the residual anomaly data, apparent density calculation, and anomaly edge detection

using Tilt Derivative (TDR), Horizontal Derivative of the Tilt Derivative (HD_TDR), Horizontal Gradient (HG), and Cos Theta map (TM). Depth Calculation was performed using Euler Deconvolution (ED) and Direct Source Parameter Imaging (DSPI). These steps are discussed below.

2.1 Terrane Correction (TC)

The study area is characterized by hills and mountains in the eastern part. Terrane correction was therefore necessary to remove the relief effect from the gravity data in order to obtain Complete Bouguer Anomaly (Kearey et al., 2002). In Oasis Montaj, terrane corrections are performed by using a combination of methods described by Kane (1962) and Nagy (1966). The associated algorithm sums the effects of four sloping triangular sections, which describe a surface between the gravity station and the elevation at each diagonal corner. In the intermediate zone, the terrain effect is calculated for each point using the flat-topped square prism approach (Nagy, 1966). In the far zone, (greater than 16 cells), the terrain effect is derived based on the annular ring segment approximation to a square prism (Kane, 1962).

2.2 Bouguer Anomaly (BA)

Bouguer correction accounts for the gravitational effects of the rocks present between the observation point and the datum (Kearey et al., 2002), the Bouguer Correction was subtracted from the FAA data to obtain the BA data of the study area. TC was then added to the BA data to obtain the CBA. The obtained CBA was gridded using the minimum curvature method utilizing a grid cell size of 100 to obtain the CBA Grid map of the area. The CBA grid map is a combination of regional anomaly, residual anomaly, and noises (Siombone et al., 2022).

2.3 Separation of Residual Anomaly, Regional Anomaly, and Noise.

In gravity surveying, it is the local anomalies that are of prime interest and the first step in interpretation is the removal of the regional field to isolate the residual anomalies (Kearey et al., 2002).

The removal of the regional field and noise to isolate the residual anomaly was done using interactive spectrum filters, specifically the Butterworth Bandpass filter. This filter separates the residual anomaly from the regional anomaly and noise simultaneously. The Butterworth Bandpass uses a central filter wavelength cutoff to isolate the residual anomaly from the regional field and noise. The central filter wavelength for residual anomaly, regional field, and noise were calculated using the following formula:

$$\text{Filter central wavelength} = \frac{1}{\text{Cutoff wave number } ({}^{1}/_{\text{k\_unit}})}$$

The filter central wavelength of 10000 m was used to isolate residual anomaly from regional anomaly, while 1670 m was used as the cutoff wavelength for noise.

2.4 Local Density Estimation

Local Density (Background Density) is equal to the average density of the dominant lithologies in the study area. According to Yadav and Sircar (2019), The local density is calculated using Nettleton's and Parasnis's method of Density calculation, where the following equation is used:

$$FAA=\rho(0.04191h-TC/2.67)$$

Using excel, FAA is plotted against 0.04191h-TC/2.67 in a scatter diagram, the slope is then calculated which is equal to the local density (ρ) in g/cm^3 of the study area. Here FAA is the Free Air Anomalies in mGal, ρ is the Local density in g/cm^3, h is the elevations in meters, and TC is the Terrane Correction in mGal. The value 2.67 g/cm^3 is the Earth's average terrane density, and 0.04191 is a Constant value.

2.5 Apparent Density Mapping

Apparent density mapping assumes a simple model layer of fixed thickness and varying density to explain an observed gravity field. The response is assumed to be caused by a collection of vertical, square-ended prisms of infinite depth extent, the horizontal dimensions of which are equal to the input grid cell size (Seequent, 2023).

The residual anomaly data is downward continued before applying an apparent density filter to close the top surface of the source model (Kearey et al., 2002). The residual

anomaly data of the study area was downward continued to 300 m, the distance at which the data shows fluctuations. The apparent density mapping by applying an inverse density deconvolution filter to the short wavelength (residual anomaly) gravity component gives density values for the upper crust which correspond well with averaged density values from rock samples (Granser et al., 1989). The apparent density map obtained was used to distinguish between metallic mineral deposits and non-mineralized intrusions in the study area.

2.6 Tilt Derivative (TDR) and its Horizontal Derivative (HD_TDR)

The TDR and HD_TDR are useful for mapping shallow basement structures and mineral exploration targets. The TDR produces sharp anomalies and generates a better definition of the edge over the geological body (Verduzco et al., 2004). The HD_TDR produces high anomalies along the faults and contacts of the geological bodies.

The tilt angle function is given by the arctangent of the ratio of the vertical derivative (VDR) of the potential field to the HG, the tilt amplitude variation has the range between $-\pi/2$ and $\pi/2$ according to the nature of the arctangent trigonometric function (HG) (Ibraheem et al., 2019):

$$TDR = \theta = \frac{VDR}{HG}$$

The TDR amplitude has a positive value over the source, zero at the edge, and negative outside the source (Ibraheem et al., 2018).

The HD_TDR is defined as:

$$HD\_TDR = \sqrt{\left(\frac{dTDR}{dx}\right)^2 + \left(\frac{dTDR}{dy}\right)^2}$$

The TDR and HD_TDR were used to define the faults or contacts and the shape of the residual anomaly bodies, such as intrusions in the study area.

2.7 Horizontal Gradient (HG)

The HG was used to map shallow faults and contacts in the study area. The HG is less sensitive to noise and also robust in the detection of shallow sources (Phillips, 2002). It shows maximum values over the faults and edges of the anomalous bodies, especially when the edges are vertical and well separated (Cordell & Grauch, 1985). The HG is determined by the following equation:

$$HG = \sqrt{\left(\frac{dF}{dx}\right)^2 + \left(\frac{dF}{dy}\right)^2}$$

Where dF/dx and dF/dy are the two horizontal derivatives of the observed fields.

2.8 Theta Map (Cos (θ))

In the Theta map, the sources situated at different depths produce similar amplitude even though the response from deeper sources is more diffuse (Cooper & Cowan, 2006). The Theta map is used to detect edges regardless of the strike and amplitude of the anomaly source (Oruç & Keskinsezer, 2008). It is calculated using the formula below:

$$\text{Cos}\,(\theta) = \frac{\text{Horizontal Gradient (HG)}}{\text{Analytical Signal (AS)}}$$

where $0 < \theta > \pi/2$ as it relies on a horizontal gradient, which is always positive (Ibraheem et al., 2019).

2.9 Euler Deconvolution (ED) method

ED is applied to the residual anomaly map to locate contacts and faults with their respective depths (Ibraheem et al., 2019). The structural index SI=0 was selected, with a maximum depth tolerance of 5% and a window size of 10×10.

2.10 Direct Source Parameter Imaging (DSPI)

This technique was employed to calculate the depths to the top of the source bodies.

The DSPI is the inverse of the HD_TDR (Thurston & Smith, 1997; Lghoul et al., 2023). This technique uses peak values to calculate depth solutions. A peak value of 3 was used, where grid values in three directions are lower. A peak

value of 3 usually works best compared to a peak value of 1, 2, or 4 (Blakely & Simpson, 1986).

3 Results

3.1 Surface Lineaments, from Digital Elevation Model (DEM SRTM data).

The surface lineaments represent surface faults or fractures present in the area (cf. Siombone et al., 2022). The rivers and stream flow follows the faults zones, shear zones, and fractures zones. The surface lineaments in the study area are traced as white dashed lines in the DEM SRTM map (Figure. 4). The orientations of these lineaments are indicated on the rosette diagram (Figure. 5), which shows that the surface lineaments in the study area are predominantly trending in the northwest-southeast direction.

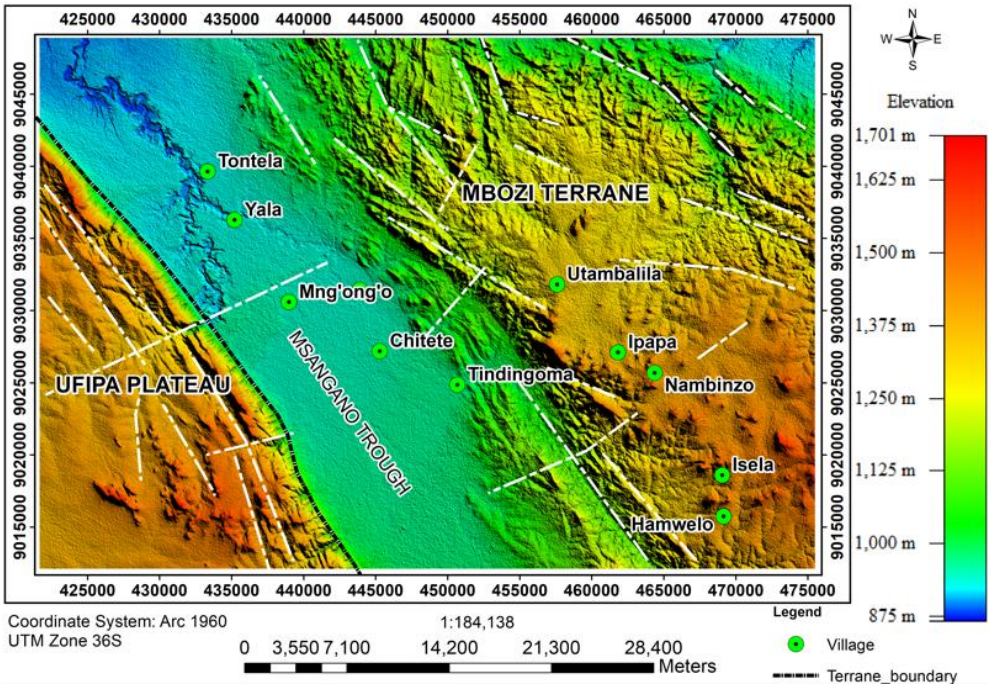

Figure. 4: Digital Elevation Model showing major surface lineaments traced as dashed white lines.

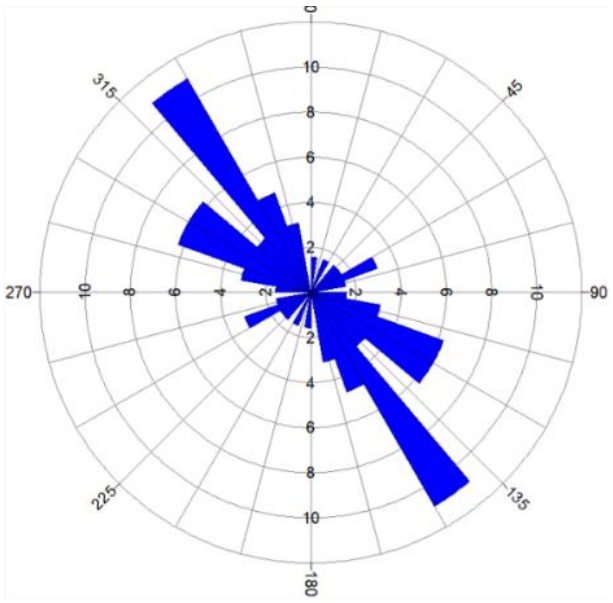

Figure. 5: Rose diagram showing the orientation of the surface lineaments in the study area.

3.2 Local Density of the Study Area The Nettleton and Parasnis graph (Figure. 6) of density calculation indicates that the study area is characterized by dense rock formations with a density value of 2.99 g/cm3. This value corresponds to the density of basaltic rocks (Kearey et al., 2002; Yadav & Sircar, 2019), which aligns with the geology of the study area (Mbozi terrane). The Mbozi terrane predominantly consists of Paleoproterozoic meta basalts (Boven et al., 1999; Boniface, 2009).

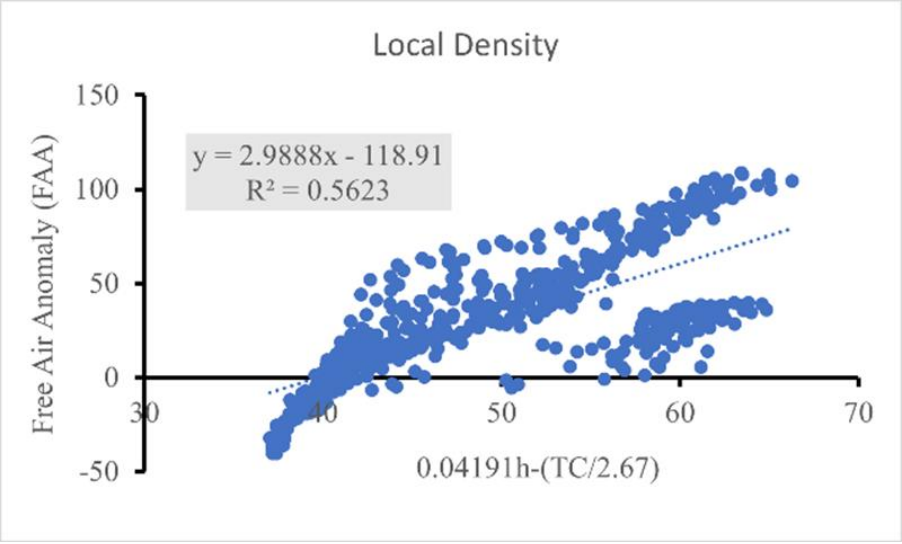

Figure. 6: The Parasnis and Nettleton graph showing the local density of the study area. The local density is equal to the slope from the graph (2.9888 g/cm3).

3.3 Complete Bouguer Anomaly (CBA) map.

The CBA map (Figure. 7) is the combination of regional anomaly, residual anomaly, and noise of the study area. Consequently, it is used solely for the general interpretation of the study area. The map indicates that the Mbozi block predominantly exhibits high Bouguer anomalies (Red colors) ranging from -102.43 to -57.48 mGal, The Msangano Trough is characterized by medium Bouguer anomalies (green) with values ranging from -122.46 to -102.43 mGal, While, the Ufipa Plateau shows low Bouguer anomalies (Blue) ranging from -157.68 to -122.46 mGal. These differences in anomalies reflect variations in the lithological densities and depths between the Mbozi block and the Msangano Trough.

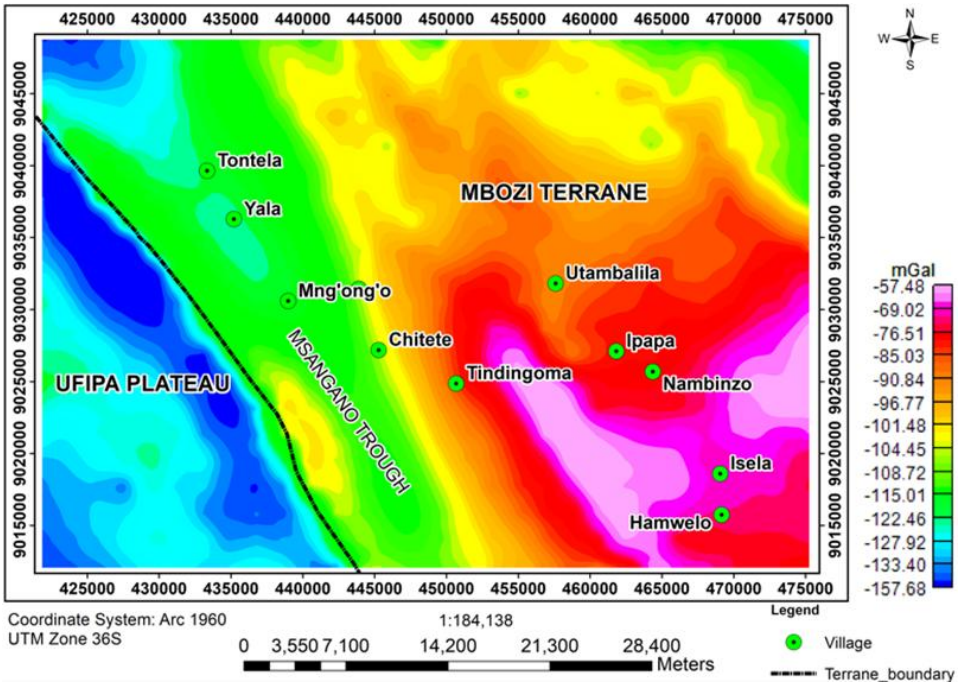

Figure. 7: The Complete Bouguer Anomaly map of the study area.

The high anomalies in the Mbozi block suggests the presence of high-density rocks (meta-basalts). the low anomalies in the Msangano Trough are due to the occurrence of the Mughese shear zone beneath it and the accumulation of Late Cenozoic sediments. In contrast, the Ufipa terrane is dominated by gneissic granite (Daly, 1988), the gneissic granites possess lower density value as compared to meta-basalts rocks (Kearey et al., 2002; Yadav & Sircar, 2019). Therefore, the Ufipa plateau shows low Bouguer Anomaly as compared to the Mbozi terrane. The boundary between the high anomalies (Red) and low anomalies (Blue) indicates the rift structures. The Msangano trough is the rift structure which cut the Mbozi terrane, it separates the high anomaly Mbozi block from low anomaly Ufipa plateau.

3.4 Regional Bouguer Anomaly map

The regional Bouguer Anomaly describes the conditions of the basement structures and is related to the depth changes and density of the basement rocks in the study area (cf. Meilasandi et al., 2019; Siombone et al., 2022).

The regional Bouguer Anomaly map (Figure. 8) of the study area indicates high regional Bouguer Anomaly values ranging from -101.07 to -61.12 mGal in the Mbozi block and low regional Bouguer Anomaly values ranging from -145.74 mGal to -101.07 mGal in the Msangano Trough and Ufipa plateau. This form of anomaly suggests

that the bedrocks in the Mbozi block (meta basalts) are (granitic gneisses). denser as compared to the bedrocks in the Ufipa plateau

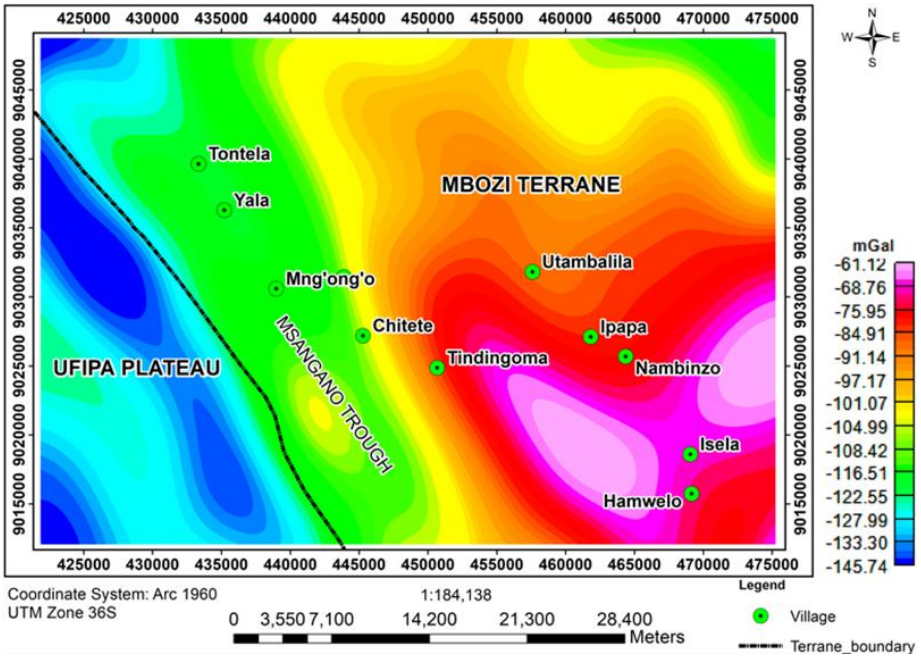

Figure. 8: Regional anomaly map showing the condition of the basement rocks in the study area.

The Radially averaged power spectrum (Figure. 9) indicates that the basement rocks in the study area are situated at an average depth of 5.2 km below the surface.

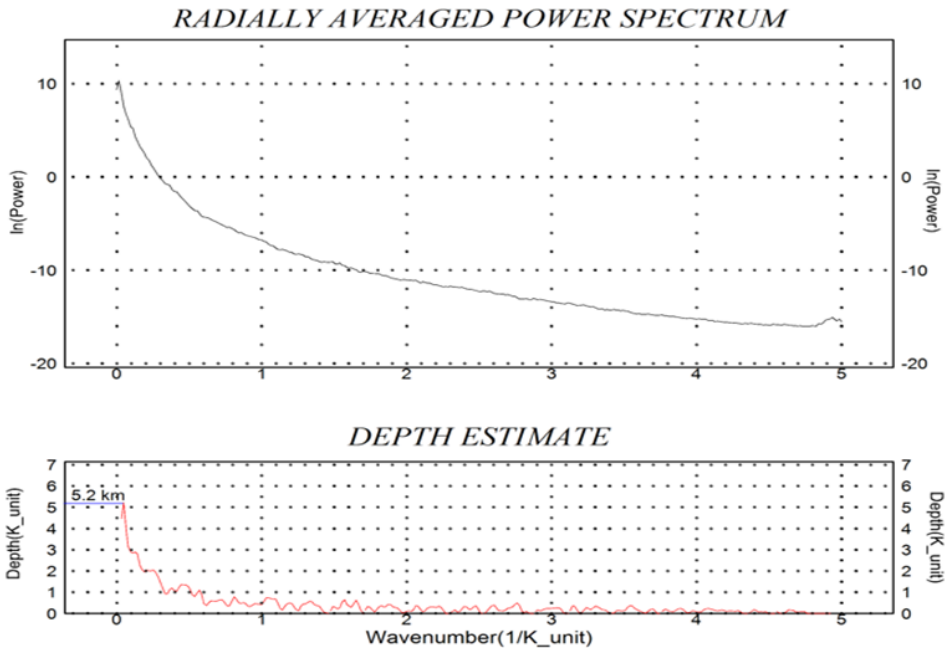

Figure. 9: Radially averaged power spectrum showing depth estimate to the basement rocks.

3.5 Subsurface Geology, from Residual Bouguer Anomaly map.

Residual Bouguer Anomaly describes the local geology of the area, with anomalies related to the subsurface structures. The residual Bouguer Anomaly map (Figure. 10) of the study area indicates the occurrence of northwest-southeast trending positive anomalies (Red colors), with values ranging from 0.27 to 11.36 mGal. In contrast, the negative residual Bouguer Anomaly values range from -14.97 to -0.08 mGal. The high residual anomalies indicate zones of high-density rocks (meta-basalts), intrusions or mineral deposits. The negative anomalies indicate zones with low-density rocks, such as shear zones, Alteration zones, grabens, or small basins. The boundary between low anomaly and high anomalies indicates lithological contacts or faults.

Two intrusions with the highest residual Bouguer Anomaly values ranging from 3.01 to 11.36 mGal are observed in the Msangano trough (Figure. 10). The larger deposit strike in the northwest-southeast direction along the terrane boundary in the Msangano trough, it is on the west of the Tontela, Yala, and Mng'ong'o villages. The smaller deposit run from East of the Tindingoma village to the West of the Hamwelo village. The exceptionally high residual anomaly value of these two bodies indicates that they are denser than all other intrusions in the study area. Additionally, the negative anomaly zones adjacent and parallel to these intrusions suggests the presence of alteration zones.

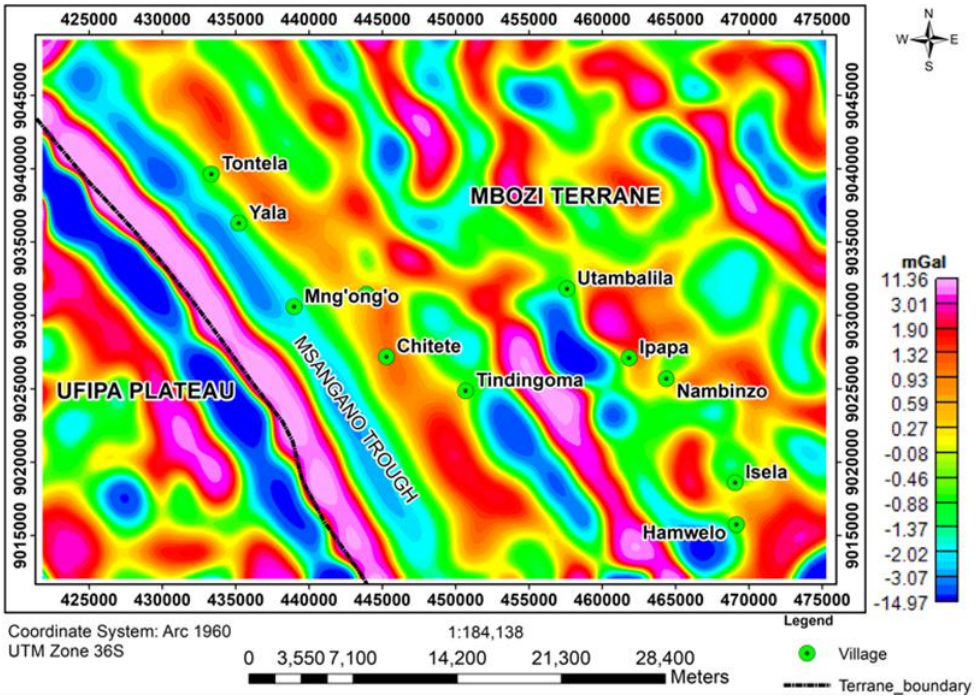

Figure. 10: Residual Bouguer anomaly map showing the subsurface geology of the study area.

3.6 Apparent Densities of the Intrusions.

The Apparent density map (Figure. 11) indicates that the Density values of the positive residual Bouguer anomalies in the study area range from 2.99 to 4.30 g/cm^3. This suggests the presence of metamorphic rocks, igneous intrusions, and metallic mineral deposits. In contrast, the density values of negative residual Bouguer anomalies range from 1.11 to 2.78 g/cm^3, indicates the presence of buried grabens, alteration zones, sheared zones, fractured zones, faults zones, trough, water saturated zones or

aquifers and basins, for instance Utambalila-Ipapa basin (Known as Kwibonde by the resident Nyiha and Nyamwanga people) which is the main area for cultivation of rice in the Mbozi district.

The two positives residual Bouguer Anomaly intrusions occurring in the Msangano trough show the highest density values, ranging from 3.62 to 4.30 g/cm^3, which are typical density values of metallic mineral deposits, because only metallic mineral deposits can have density values greater than 3.54 g/cm^3 density of Eclogite. The larger deposit strike in the northwest-southeast direction along the terrane boundary in the Msangano trough. The smaller deposit runs from East of the Tindingoma village to the West of the Hamwelo village.

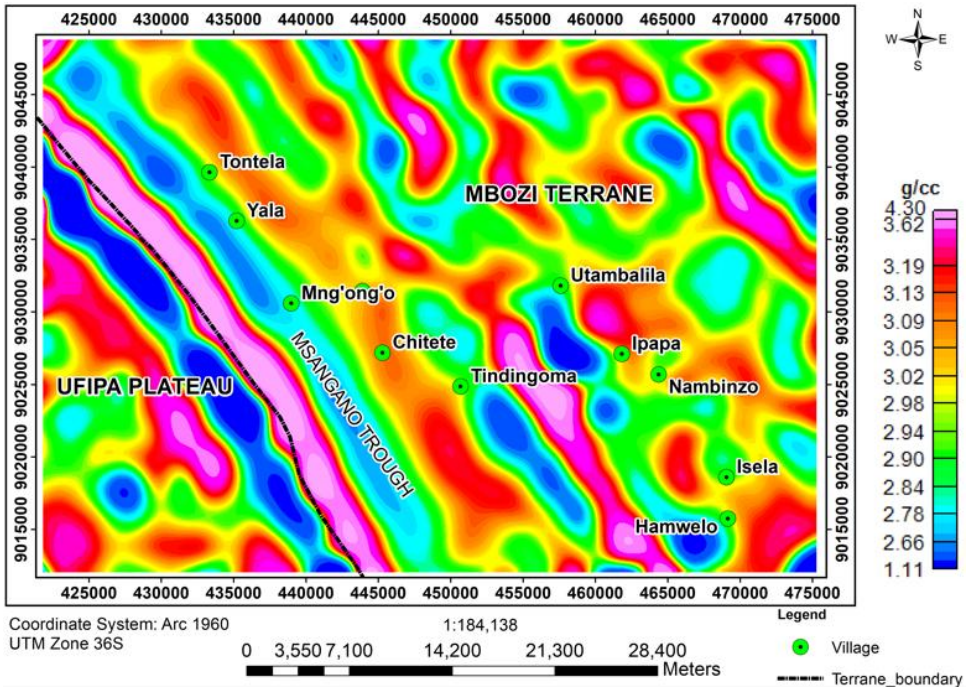

Figure. 11: Apparent density map, showing the density of the residual Bouguer anomalies in the study area.

3.7 Subsurface Faults and Geological Contacts, from Edge Detectors.

The subsurface faults and edges of the geological bodies in the study area were identified from several edge detector maps, such as the Theta map, HG map, TDR map, and HD_TDR map. Each of these maps is described below.

- **Theta map and Horizontal Gradient (HG) map**

All the geological contacts and major subsurface faults in the study area are indicated as linear features of high anomalies ranging from 0.7821 to 1.0049 radians, in the Theta map (Figure. 12). These faults and contacts are identified regardless of their orientation and depth. However, Theta map cannot distinguish faults from contacts.

The HG map, along with the TDR map and HD_TDR map, was used to distinguish faults from contacts. The HG map (Figure. 13) indicates shallow faults as high gradients linear anomalies ranging from 0.001359 to 0.015893 mGal/m, while deep faults are indicated as low gradient anomalies of less than 0.000541 mGal/m. Very high gradient anomalies due to density contrast, ranging from 0.004574 to 0.015893 mGal/m are observed over the edges of the high-density body within the Msangano Trough.

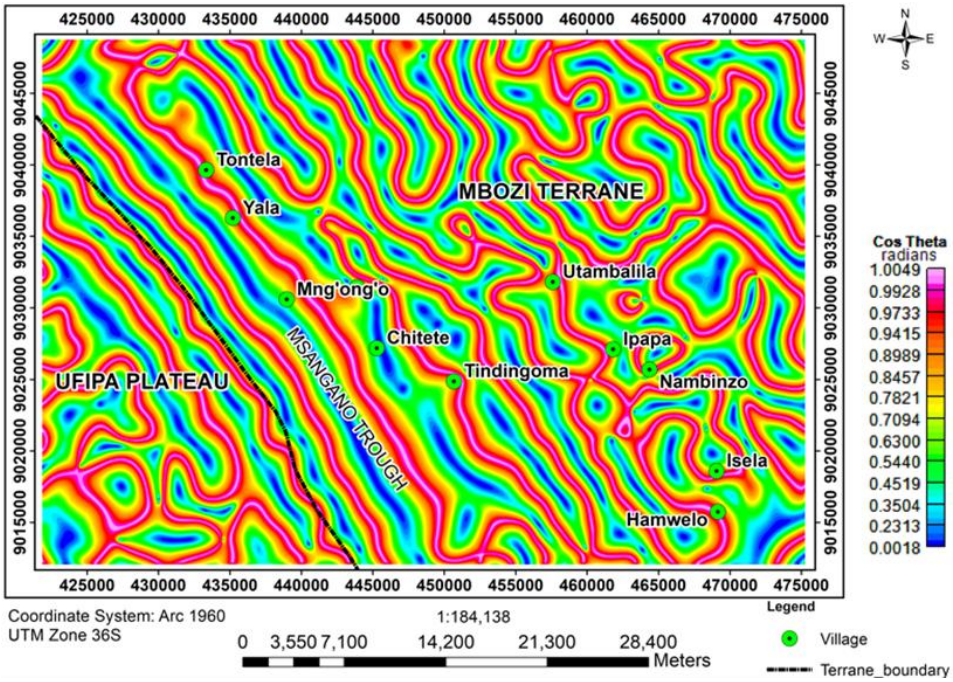

Figure. 12: Theta map of the study area showing the subsurface faults and geological contacts as high linear anomalies.

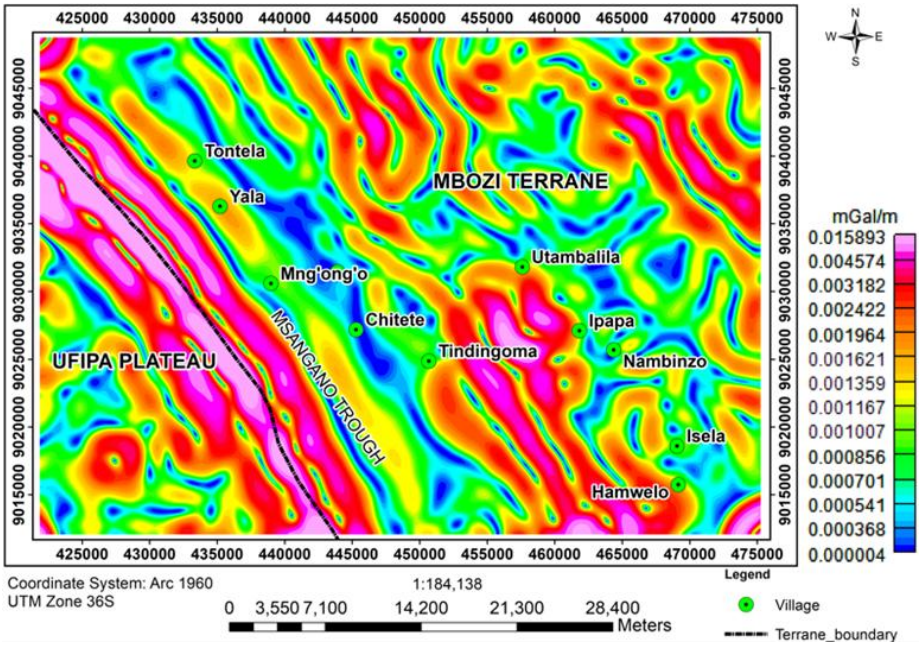

Figure. 13: HG map showing the shallow faults (high anomalies) and deep faults (low anomalies).

Tilt Derivative (TDR) and its Horizontal Derivative (HD_TDR) map

The TDR map (Figure. 14) defines edges over the geological bodies, indicating the shape and size of the residual Bouguer anomalies in the study area.

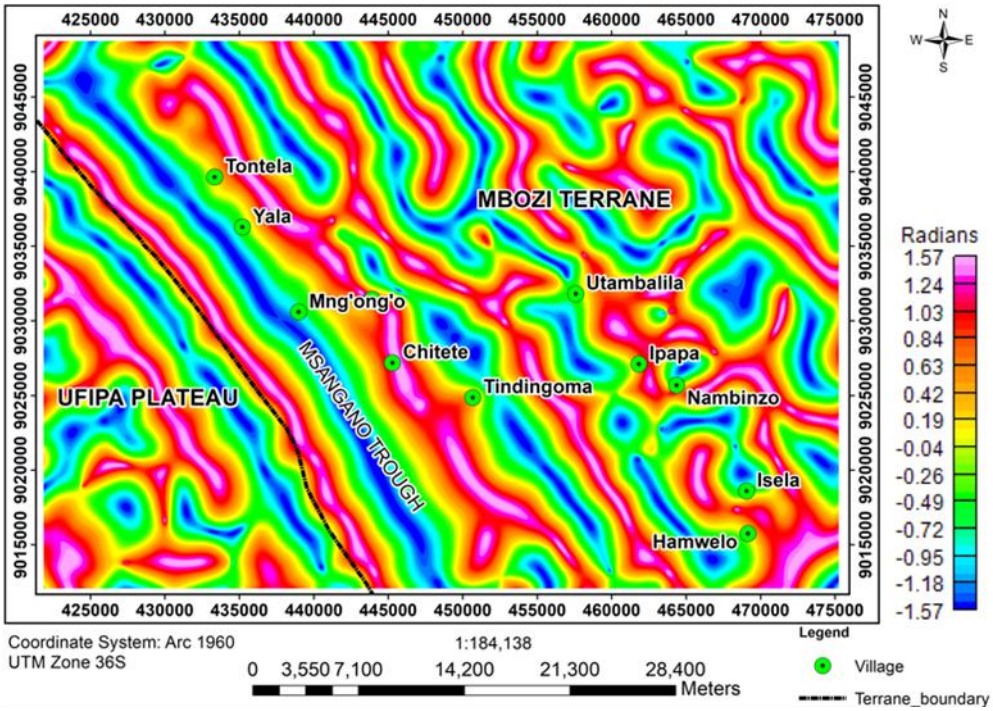

Figure. 14: Tilt derivative (TDR) map of the study area showing the shape and sizes of the anomalies.

The HD_TDR map (Figure. 15) indicates geological contacts, faults, basins, grabens, and Trough present in the study area. The lithological contacts and faults are indicated as high anomalies (red). In contrast, the basins, grabens, and Trough show a wide distribution of low anomalies (blue and green colors). For instance, widely distributed low anomalies occur within the Msangano Trough.

The HD_TDR map is also used in determining the fault dip direction. The high anomalies (red) occurring adjacent to the distributed low anomalies indicates faults. In contrast, the high anomalies adjacent to each other represent or indicates lithological contact. The faults dips toward the distributed low anomalies (blue).

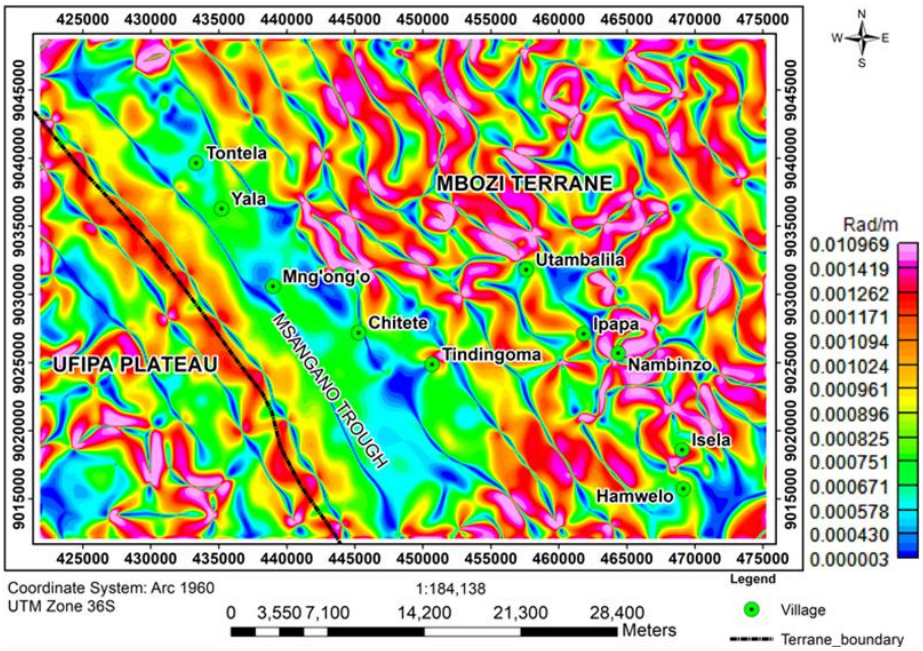

Figure. 15: HD_TDR map showing faults, contacts (high anomalies), and subsidence zones (distributed low anomalies)

3.8 Depths to the Anomalies

The depths to the anomaly bodies were estimated from Euler deconvolution (ED) and Direct Source Parameter Imaging.

- **Euler deconvolution**

The structural index S=0, maximum depth tolerance of 5% and window size of 10 × 10 was used in ED to estimate the locations of the faults and their depths. The ED (Figure. 16) indicates that the faults in the study area are shallow, located at varying depths from 297 m to 1.94 km below the surface.

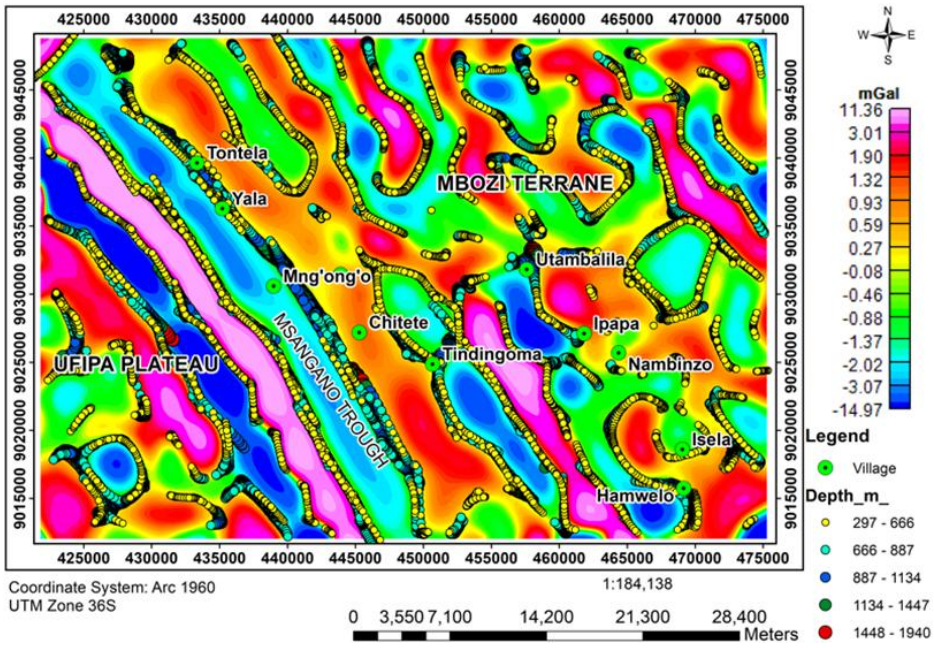

Figure. 16: The ED solutions superimposed on the residual anomaly map of the study area to locate contacts and faults with their respective depths.

- **Direct Source Parameter Imaging**

The DSPI estimated the depths to the top of the residual Bouguer Anomaly bodies or intrusions. The DSPI in Figure. 17 indicates that the anomaly source bodies in the study area are located at a depth ranging from 89 m to 3.33 km below the surface. The DSPI shows that the metallic mineral deposits in the Msangano trough are situated at a depth ranging from 796 m to 1.17 km beneath the Late Cenozoic sediments which covers the Msangano trough. The basement rocks in the Msangano trough are buried at a depth varying from 1.17 km to 2.1 km beneath the late Cenozoic sediments. The deepest source body in the study area is located on the southeast of the Hamwelo village at a depth of 3.33 km below the surface.

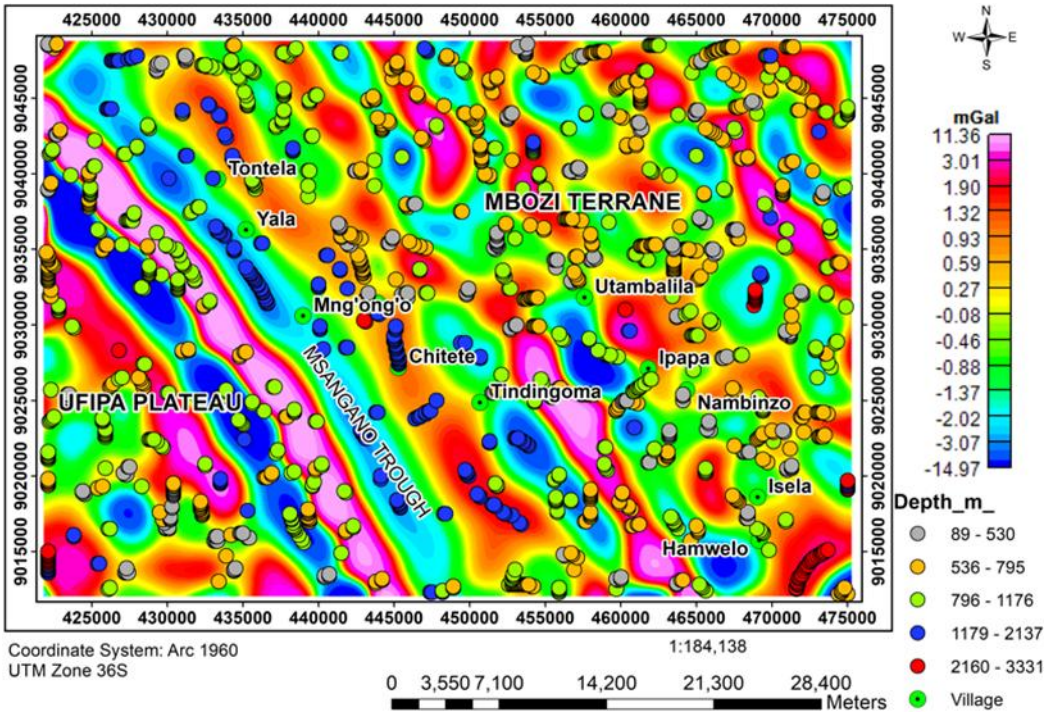

Figure. 17: The DSPI solutions are superimposed on the residual anomaly map to indicate depths to the intrusions (high residual anomalies), and negative residual anomalies.

3.9 Deduced Subsurface Structural map

Only subsurface geological structures confirmed by all the employed methods were chosen to construct the subsurface structural map of the study area.

The deduced structural map (Figure. 18) indicates the two metallic mineral deposits (A and B) present in the study area. The deposits are highlighted in yellow. The larger deposit A spans 109.8 km^2, while the smaller deposit B covers 62.2 km^2. The map reveals that the study area is structurally controlled by several faults, predominantly trending in the northwest-southeast direction, as supported by the Rose diagram (Figure. 19). Additionally, the map shows the presence of buried grabens, caused by the subsidence of several dense blocks in the Mbozi terrane and Ufipa Plateau.

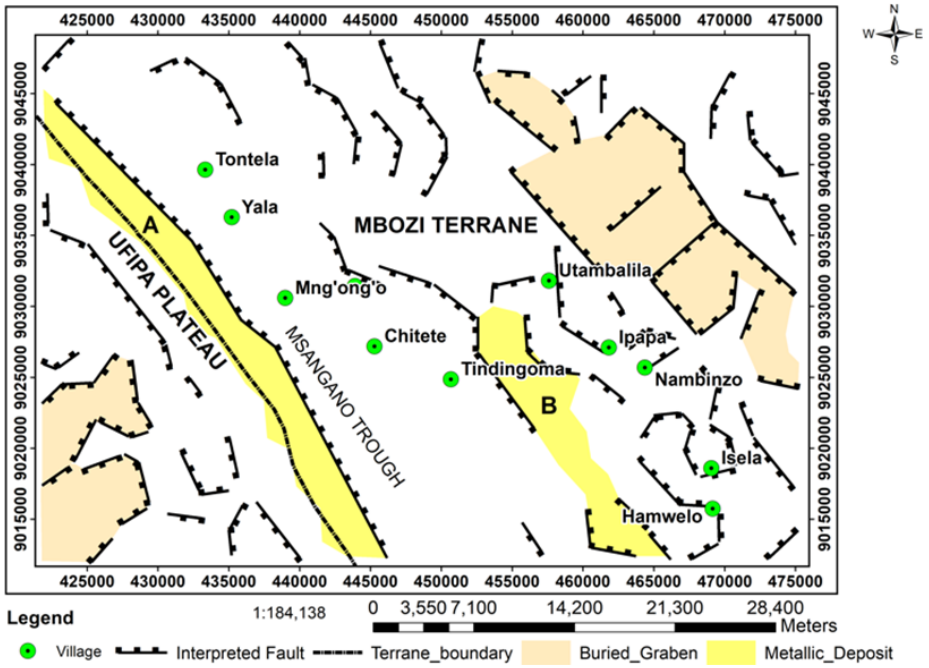

Figure. 18: Deduced subsurface structural map showing dip direction of the interpreted faults, Location of the two metallic mineral deposits (A and B), and buried grabens present in the study area.

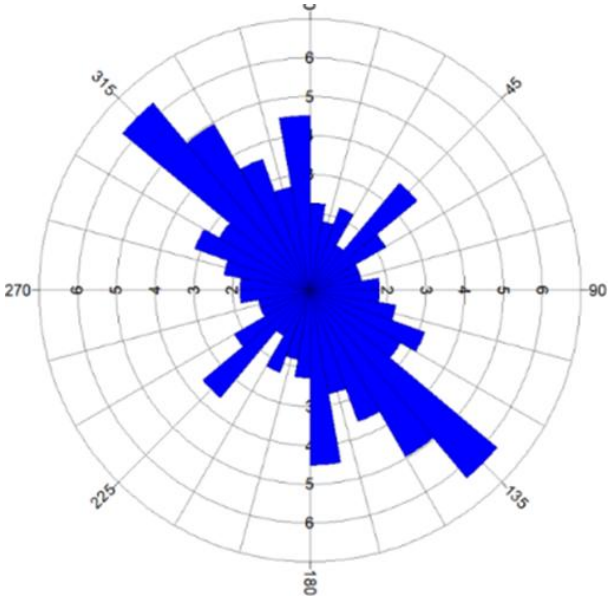

Figure. 19: Rose diagram showing the orientation of the interpreted faults in the study area.

4 Discussion

The regional Bouguer Anomaly map (Figure. 8) indicates that the basement rocks in the Mbozi block and Msangano Trough are located at a deeper level compared to the basement rocks in the Ufipa plateau. The average power spectrum (Figure. 9) suggests that the average depth to the basement rocks in the study area is 5.2 km below the surface.

The residual Bouguer Anomaly data and DSPI (Figure. 17) indicate that the study area is dominated by mafic

intrusions located at varying depths ranging from 89 m to 3.3 km below the surface. These intrusions are of Paleoproterozoic age (Boven et al., 1999; Boniface, 2009). The Paleoproterozoic rocks were later cut by northwest-southeast trending Cenozoic faults (Morley et al., 1992) which provided the pathway for the deposition of metallic mineral deposits within the Msangano Trough. The Euler deconvolution (Figure. 16) indicates that these Cenozoic faults in the study area are shallow, located at varying depths ranging from 297 m to 1.94 km below the surface.

The deduced structural map (Figure. 18), indicates the presence of buried grabens in the northeastern and southwestern parts of the study area. The grabens were created by the subsidence of dense blocks due to Cenozoic faulting.

The apparent density data (Figure. 11) indicates that the metallic mineral deposits in the Msangano Trough have an average density value ranging from 3.62 to 4.30 g/cm^3. Figure. 18 indicates that the two deposits A and B are 109.8 km2 and 62.2 km^2, respectively. The geology of the study area, predominantly consisting of meta-basalts, suggests that these metallic mineral deposits are associated with mafic intrusions. The mafic-related deposits are known for hosting Ni and PGE ore minerals (Wadsworth et al., 1982). The DSPI (Figure. 17) indicates that these deposits are situated at an average depth of 950 m beneath the late Cenozoic sediments within the Msangano Trough.

The deposits A and B in the Msangano trough (Figure. 18) exhibit characteristics that draw compelling comparisons to other significant mafic mineral deposits in Tanzania and Worldwide. The comparisons in age, and size to other notable mafic mineral deposits including the Kapalagulu layered mafic igneous complex in western Tanzania, the Bushveld Igneous Complex (BIC) in South Africa, the Sudbury complex in Ontario, Canada, and the Zimbabwe Great dyke, are detailed and discussed below.

Kapalagulu layered mafic igneous complex in western Tanzania: This complex dates back to 1392 ± 26 million years, it spans an area of 23 km^2 (Maier et al., 2007). This complex is younger compared to the 1977 ± 40 million years age of mafic intrusions in the Mbozi terrane (Boven et al., 1999; Boniface, 2009). Additionally, the Kapalagulu complex is smaller in size compared to the deposits A and B in the Msangano Trough, which cover areas of 109.8 km2 and 62.2 km^2, respectively.

Bushveld Igneous complex (BIC) in south Africa: This complex contains the world greatest reserve of chromium and platinum group metals (PGM). The complex spans an area of 67,000 km^2 and dates back approximately 1.9 billion years (Eriksson et al., 1995), similar to the 1977 ± 40 million years of age of the meta basalts in the Mbozi terrane (Boven et al., 1999; Boniface, 2009). The BIC consist of a layered igneous structure with more mafic, magnesium-chromium rich rocks at the base.

Sudbury Complex in Ontario, Canada is renowned as the world's most productive source of nickel deposits. The Sudbury Complex occurs in an elliptical depression 60 km long by 30 km wide, with the long axis trending east-northeast. It is dated back between 1.7 to 2.0 billion years (Therriault et al., 2002), similar to the 1977 ± 40 million years age of mafic intrusions found in the Mbozi terrane (Boven et al., 1999; Boniface, 2009).

Zimbabwe Great Dyke is a layered igneous complex containing large reserve of stratiform chromite. It stretches 532 km long and ranges from 5 to 9.5 km wide. The age of the complex is about 2.5 billion years (Mukasa et al., 1998), which is older than the meta basalts in the Mbozi terrane.

The clear similarity in age among the mafic rocks in the Mbozi terrane, the Bushveld Igneous Complex, and the Sudbury Complex in Ontario, Canada, is noteworthy. This alignment in age suggests that the Msangano deposits in the Msangano trough Mbozi terrane, along with the Bushveld Igneous Complex and the Sudbury Complex, share the same worldwide magmatic events that occurred during the Paleoproterozoic era.

The fact that these magmatic events enriched the Bushveld Igneous Complex with Chromium and Platinum Group Metals, and the Sudbury Complex with nickel, indicates a significant potential for the Msangano

deposits. It implies that the Msangano deposits could also be enriched with valuable elements such as Nickel, Chromium, or Platinum Group Metals.

By drawing these parallels, it becomes evident that the Msangano deposits hold promising prospects for mineral wealth, similar to those found in the Bushveld Igneous Complex and the Sudbury Complex. Conducting detailed high resolution airborne magnetic surveys over these deposits is therefore crucial. These surveys can provide more precise data, leading to improved targeting of the Msangano mineral deposits

Apparent density mapping techniques and edge detection using free TOPEX satellite data are highly recommended for use in other regions to facilitate the discovery of mineral deposits. These methods can effectively narrow down target areas for mineral prospecting prior to detailed exploration, thereby reducing the financial costs associated with metallic mineral exploration.

5 Conclusion

This study used combined geophysical approach involving interpretation of TOPEX gravity satellite and Digital Elevation Model from the Shuttle Radar Topography Mission (DEM SRTM) datasets to conclude the following for the Msangano Trough, Mbozi Terrane, Tanzania:

- The study area contains two potential metallic mineral deposit sites (A and B) covering 109.8 km^2 and 62.2 km^2, respectively.
- Both deposits (A and B) are structurally controlled, situated within northwest-southeast trending fault zones and shear systems dissecting the study area.
- Intrusion of mafic igneous bodies is believed to have played a key role in the emplacement of these deposits.
- The identified metallic mineral deposits indicate a promising region for the exploration and prospecting of mafic related metallic minerals such as chromium, nickel or platinum group metals.

Acknowledgment

The Author wishes to express gratitude to the National Aeronautics and Space Administration (NASA), and the United States Geological Survey (USGS) for generously providing the TOPEX gravity data and DEM SRTM at no cost, which significantly facilitated this work.

Conflict of Interest

The Author declares no conflict of interest.

Funding Status

This work received no fund.

Data availability Statement

The TOPEX gravity data used in this study is available via link: https://topex.ucsd.edu/cgi-bin/get_data.cgi

The DEM SRTM data is available via link: https://earthexplorer.usgs.gov/.

References

Blakely, R. J., & Simpson, R. W. (1986). Approximating edges of source bodies from magnetic or gravity anomalies. *Geophysics* 51(07): 1494-1498).

Boniface, N. (2009). Eburnian, Kibaran, and Pan-African metamorphic events in the Ubendian belt of Tanzania: Petrology, Zircon and Monazite Geochronology (Doctoral Dissertation, Christian-Albrechts Universität Kiel).

Boven, A., Theunissen, K., Sklyarov, E., Klerkx, J., Melnikov, A., Mruma, A., & Punzalan, L. (1999). Timing of exhumation of a high-pressure mafic granulite terrane of the Paleoproterozoic Ubende belt (West Tanzania). *Precambrian Research,* 93: 119-137.

Cooper, G., & Cowan, D. (2006). Enhancing potential field data using filters based on the local phase. *Comput. Geosci.* 32: 1585–1591.

Cordell, L., & Grauch, V. (1985). Mapping basement magnetization zones from aeromagnetic data in the San Juan basin, New Mexico. In Hinze WJ (Ed)The Utility of Regional Gravity and Magnetic Anomaly Maps (pp.181-197).

Daly, M. (1988). Crustal Shear Zones in Central Africa: a Kinematic Approach to Proterozoic Tectonics. *Episodes* 11(1): 5-11).

Damblon, F., Gerrienne, P., D'Outrelepont, H., Delvaux, D., Beeckman, H., & Back, S. (1998). Identification of a fossil wood specimen in the Red Sandstone Group of southwestern Tanzania: stratigraphic and tectonic implications. *Journal of African Earth Sciences*, 26: 387–396.

Delvaux, D., Kervyn. F., Macheyeki, A., & Temu, E. (2012). Geodynamic Significance of the TRM Segment in the East African Rift (W-Tanzania): Active Tectonics and Paleostress in the Ufipa Plateau and Rukwa Basin. *J. Struct. Geology*, 37: 161–180.

Eriksson, G., Hattingh, J., Altermann, W. (1995). An overview of the geology of the Transvaal Sequence and Bushveld Complex, South Africa. *Mineralium Deposita* 30(2): 98-111.

Gilbert, J., & Park, C. F., Jr. (2007). The Geology of Ore deposits. Waveland Press.

Granser, H., Meurers, B., & Steinhauser, P. (1989). Apparent Density Mapping and 3D Gravity Inversion in the Eastern Alps. *Geophysical Prospecting*, 37: 279-292.

Grantham, D. (1931). Lupa River Goldfield. *Mining Magazine*, 265-276.

Ibraheem, I.M., Haggag, M., & Tezkan, B. (2019). Edge Detectors as Structural Imaging Tools Using Aeromagnetic Data: A Case Study of Sohag Area, Egypt. *Geosciences*, 9(211) 1-13).

Ibraheem, I., Gurk, M., Tougiannidis, N., & Tezkan, B., (2018). Subsurface investigation of the Neogene Mygdonian Basin, Greece using magnetic data. Pure *Appl. Geophys*, 175: 2955–2973.

Kane, M. (1962). A Comprehensive System of Terrain Using a Digital Computer. *Geophysics*, 27(4): 455-462).

Kearey, P., Brooks, M., & Hill, I. (2002). An Introduction to Geophysical Exploration (3rd ed.). Blackwell Science.

Kilembe, E.A., & Rosendahl, B.R. (1992). Structure and stratigraphy of the Rukwa rift. *Tectonophysics*, 209: 143-158.

Kolawole, F., Jackson, CA-L., Atekwana, E., & Philips, T. (2021). Structural Inheritance Controls Strain Distribution During Early Continental Rifting, Rukwa Rift. *Front. Earth Sci*., 9: 707869.

Lawley, C.J., Imber, J., & Condon, D.J. (2014). Palaeoproterozoic orogenic gold style mineralization at the southwestern Achearn Tanzania Cratonic margin, Lupa Gold Field, SW Tanzania: Implication from U-Pb titanite geochronology. *Gondwana Research*, 26: 1141-1158.

Lemna, O., Stephenson, R., & Cornwell, D. (2019). The Role of Pre-Existing Precambrian Structures in the Development of Rukwa Rift Basin, Southwest Tanzania. *J. Afr. Earth Sci*, 150: 607–625.

Lenoir, J., Liégeois, J.-P., Theunissen, K., & Klerkx, J. (1994). The Paleoproterozoic Ubendian Shear belt in Tanzania: Geochronology and Structure. *J. Afr. Earth Sci.* 19(3):169–184).

Lghoul, M., Abd-Elhamid, H.F., Zelenakova, M., Abdelrahman, K., Fnais, M.S., & Sbihi, K. (2023). Application of enhanced methods of gravity data analysis for mapping the subsurface structures of the Bahira basin in Morocco. *Front. Earth Sci*, 11: 1225714.

Maier, D., Peltonen, P., & Livesey, T. (2007). The ages of the Kabanga North and Kapalagulu intrusions, western Tanzania: A reconnaissance study. *Economic Geology*, 102(1): 147-154).

Meilasandi, T., Sugianto, A., Indriana, R., & Harmoko, U. (2019). 3D Gravity Data Modelling for Determining a Subsurface Structure of The SDP Geothermal Field. *Journal of Physics: Conference Series*, 1217: 012042.

Morley, C., Cunningham, S., Harper, R., & Wescott, W. (1992). Geology and Geophysics of the Rukwa Rift, *East Africa. Tectonic,* 11(1: 69-81).

Mukasa, B., Wilson, H., & Carlson, W. (1998). A multielement geochronologic study of the Great Dyke, Zimbabwe: significance of the robust and reset ages. *Earth and Planetary Science Letters*, 164: 353-369.

Nagy, D. (1966). The Gravitational Attraction of a Right Rectangular Prism. *Geophysics*, 31(2): 362-371).

Oruç, B., & Keskinsezer, A. (2008). Structural setting of the northeastern Biga Peninsula (Turkey) from tilt derivatives of gravity gradient tensors and magnitude

of horizontal gravity components. *Pure Appl. Geophys*, 165: 1913–1927.

Phillips, J. (2002). Processing and Interpretation of Aeromagnetic Data for the Santa Cruz Basin-Patahonia Mountains Area, South-Central Arizona. *U.S. Geological Survey* open-file report 02-98.

Pinna, P., Muhongo, S., Mcharo, B.A., Le Goff, E., Deschamps, Y., Ralay, F., & Milesi, J.P. (2004). Geology and Mineral Map of Tanzania. Geological Survey of Tanzania.

Seequent. (2023). Apparent Density Calculation (DENS). https://help.seequent.com/Oasismontaj/2023.2/Content/gxhelp/fff2con_dens.htm

Siombone, S.H., Susilo, A., & Maryanto, S. (2022). Integration of TOPEX Satellite Gravity and Digital Elevation Model Shuttle Radar Topography Mission (DEM SRTM) Imagery for Subsurface Structure Identification at Tiris Geothermal Area. *Positron* 12(2): 98-111).

Therriault, A., Fowler, A., Grieve, R. (2002). The Sudbury Igneous Complex: A Differentiated Impact *Melt Sheet* 97(7): 1521-1540).

Thurston, J.B., & Smith, R.S. (1997). Automatic conversion of magnetic data to depth, dip, and susceptibility contrast using the SPITM method. *Geophysics*, 62: 807-813.

Verduzco, B., Fairhead, J., Green, C., & MacKenzie, C. (2004). New insights into magnetic derivatives for structural mapping. *Lead. Edge*, 23: 116–119.

Wadsworth, W., Dunham, A., & Almohandis, A. (1982). Cryptic variation in the Kapalagulu layered intrusion, western Tanzania. *Mineral. Mag*, 45: 227–236.

Yadav, K., & Sircar, A. (2019). Modeling Geothermal Prospects using Gravity Data. *Dew Journal*, 87-96.